Rigorous spatial statistics for gaze patterns in scene viewing: Effects of repeated viewing

Hans A. Trukenbrod[1,2] & Simon Barthelmé[3] &
Felix A. Wichmann[4,5,6] & Ralf Engbert[1,2]

[1]University of Potsdam, Germany
[2]Bernstein Center for Computational Neuroscience Berlin, Germany
[3]Grenoble INP, France
[4]Eberhard Karls University of Tübingen, Germany
[5]Bernstein Center for Computational Neuroscience Tübingen, Germany
[6]Max Planck Institute for Intelligent Systems, Tübingen, Germany

(Version: April 7, 2017)

arXiv:1704.01761v1 [q-bio.NC] 6 Apr 2017

Draft manuscript—please do not cite without permission

Address correspondence to:
Hans Trukenbrod
Department of Psychology
University of Potsdam
Am Neuen Palais 10
D–14469 Potsdam
Germany
E-mail: Hans.Trukenbrod@uni-potsdam.de
Phone: +49 331 9772703, Fax: +49 331 9772794

Scene viewing is used to study attentional selection in complex but still controlled environments. One of the main observations on eye movements during scene viewing is the inhomogeneous distribution of fixation locations: While some parts of an image are fixated by almost all observers and are inspected repeatedly by the same observer, other image parts remain unfixated among observers even after long exploration intervals. Here, we apply spatial point processes to investigate the correlations between pairs of points. More technically, the *pair correlation function* (PCF) is a powerful statistical tool to evaluate how individual scanpaths deviate from the inhomogeneity observed across participants. We demonstrate that aggregation of fixation locations within four degrees is stronger during individual trials than expected by the inhomogeneity of the distribution. Furthermore, the PCF reveals stronger aggregation of fixations when the same image is presented a second time. We use simulations of a dynamical model to show that a reduced attentional span may explain differences in spatial correlations between first and second inspection of the same image.

Introduction

During scene viewing, fixation locations are not selected completely at random. Instead fixations cluster in specific areas while other areas remain unfixated even after long exploration intervals across observers. Most research on this inhomogeneity has tried to identify factors that contribute to the placement of fixations across trials, while statistical correlation within trials are completely ignored. Here we describe the pair correlation function (PCF) as a method from spatial point processes to describe the relationship between pairs of points during a single trial. When applied to eye movement data, the PCF indicates correlations of fixations within a trial when compared to the distribution of all fixation locations across trials. Furthermore, our results demonstrate that the PCF is sensitive to task demands like a memory manipulation and can be reproduced in our dynamical model simulations by a reduction of the attentional span when a scene is inspected a second time.

Eye movements during scene perception.

Local image features predict fixation locations during scene viewing. For example, luminance contrast and edge density attract gaze (Mannan, Ruddock, & Wooding, 1997; Reinagel & Zador, 1999; Tatler, Baddeley, & Gilchrist, 2005). The strength of the relationship for different image features, however, depends on the type of image viewed (Parkhurst, Law, & Niebur, 2002). In addition, saliency models assume that bottom-up feature-extraction is used to guide overt attention (Itti & Koch, 2001; cf., Koch & Ullman, 1985). This approach has led to a wide variety of computational saliency models (e.g., Bruce & Tsotsos, 2009; Kienzle, Franz, Schölkopf, & Wichmann, 2009; Parkhurst et al., 2002; Vig, Dorr, & Cox, 2014; Zhang, Tong, Marks, Shan, & Cottrell, 2008), which perform well when evaluated with a data set obtained under unconstrained ("free") viewing (Bylinskii et al., 2015).

Although image statistics predict the inhomogeneity of fixation locations, the strength of the underlying causal link has been called into question. Alternatively, fixations might be attracted by objects (Einhäuser, Spain, & Perona, 2008). This interpretation is supported

by the existence of a preferred viewing location close to the object center in scene viewing (Nuthmann & Henderson, 2010). A relationship that is weaker for points of highest saliency than for objects. Furthermore, combining object detectors (faces, persons, cars) and saliency computation improves prediction of fixation locations considerably (Cerf, Harel, Einhäuser, & Koch, 2007; Judd, Ehinger, Durand, & Torralba, 2009). While saliency initially referred to low-level local image features, recent saliency models extract high-level features like objects (e.g., Kümmerer, Wallis, & Bethge, 2016). Nonetheless, whether fixations are primarily attracted by low-level image features or rather by objects remains an ongoing controversy (Borji, Sihite, & Itti, 2013; Stoll, Thrun, Nuthmann, & Einhäuser, 2015; Stoll et al., 2015).

Beside the influence of local image statistics and objects, it has been known for a long time that top-down factors affect fixation locations. In his seminal work, Yarbus (1967) reported anecdotal evidence that scanpaths are influenced by the instruction given before viewing an image (see also Castelhano, Mack, & Henderson, 2009). These top-down effects are further strengthend when engaged in natural tasks like preparation of a sandwich or during tea-making (Hayhoe & Ballard, 2005; Land & Hayhoe, 2001). In natural tasks fixations generally support a smooth execution of the task and occur on objects just-in-time (Ballard, Hayhoe, & Rao, 1997) or as look-ahead fixations to inspect objects needed later during the task (Pelz & Canosa, 2001). Thus, the eyes do not necessarily fixate the most salient location but are rather directed towards informative locations that are important for task execution. Another source of top-down control comes from memory representations due to reinspection of previously seen images (Kaspar & König, 2011a, 2011b) and due to the acquired scene or world knowledge (Torralba, Oliva, Castelhano, & Henderson, 2006). Incorporating such knowledge by contextual priors, e.g., the position of a horizon, improves predictions of saliency models accordingly (Torralba et al., 2006; Judd et al., 2009).

Systematic tendencies of the eyes further contribute to the placement of fixations (Tatler & Vincent, 2008). A well-known example is the central fixation bias during scene viewing (Tatler, 2007). On average, participants prefer to fixate near the center of an image rather than towards the periphery. Another systematic tendency is the preference to execute saccades in cardinal directions during scene viewing. This effect is shaped by image features and varies systematically with the perceived horizon. Tilting an image results in an equally tilted distribution of saccade directions (Foulsham, Kingstone, & Underwood, 2008; Foulsham & Kingstone, 2010).

Finally, successive saccades are not independent. At least three oculomotor mechanisms have been proposed to influence the generation of scanpaths: inhibition of return, saccadic momentum, and facilitation of return (Smith & Henderson, 2009). Inhibition of return is believed to facilitate exploration during visual search (Klein & MacInnes, 1999) and has been suggested as a mechanism to drive attention through scenes in computational models (Itti & Koch, 2001). Inhibition of return during scene perception seems to primarily prolong saccade programming when saccades return to previously fixated locations (Hooge, Over, van Wezel, & Frens, 2005; Smith & Henderson, 2009) but seems to shape spatial dynamics of scanpaths in the long run (Rothkegel, Trukenbrod, Schütt, Wichmann, & Engbert, 2016). Facilitation of return increases the number of fixations to previously fixated parts of a scene (last and penultimate fixation) and saccadic momentum describes the tendency to continue a scanpath in the same direction as the preceding saccade (Smith & Henderson, 2009; Wilming, Harst, Schmidt, & König, 2013). Adding these oculomotor tendencies further improves the prediction of saliency models (Le Meur

& Liu, 2015)

Eye movements and long-term memory: Repeated presentation

Humans have a remarkable capacity to remember images in long-term memory (Brady, Konkle, Alvarez, & Oliva, 2008; Standing, 1973; Standing, Conezio, & Haber, 1970). These representations are not limited to the gist of a scene but include abstract representations of objects, in particular of previously fixated objects (Hollingworth, Williams, & Henderson, 2001; Hollingworth & Henderson, 2002). By viewing the same image multiple times scene memory accumulates (Melcher, 2001; Melcher & Kowler, 2001). Due to this scene-specific memories repeated presentations can be used to investigate effects of long-term memory on eye movements.

In two studies, Kaspar and König studied the interaction of bottom-up and top-down influences and long-term memories by presenting images five times. In general, fixation locations were moderately correlated between different inspections of the same image by the same participant (Kaspar & König, 2011b). Correlations were strongest for successive presentations and decreased with increasing distance between presentations. The correlation between fixation locations and low-level features, however, remained rather constant. In contrast, the number of fixated regions decreased after multiple presentations of images, as did the average number of fixations. Furthermore, saccade amplitudes were largest during the first presentation and decreased on subsequent presentations.

In a second study Kaspar and König (2011a) explored the effects of repeated presentations on top-down influences on saccade selection. Motivation (as measured via the reported interestingness of the viewed images) and a personality trait of participants (action orientation) influenced repeated viewing of images. In addition, fixation durations and variability between participants' fixation locations increased, whereas saccade frequency, saccade length, and entropy of fixation locations decreased. The authors concluded that the locus of attention became increasingly local with repeated presentations of images. Thus, participants scrutinized individual regions during later presentations. This interpretation was supported by participants' self-reports and was augmented in participants who found the images more interesting.

Research Questions

Much progress has been made to understand where observers fixate in an image. This research primarily focused on fixation locations across observers while neglecting the fixation history during a trial of a single observer. Fixation locations, however, exhibit strong spatial correlations during a trial and are not independent of one another (Engbert, Trukenbrod, Barthelmé, & Wichmann, 2015) and adding mechanisms that generate more realistic scanpaths improves performance of saliency models (Le Meur & Liu, 2015). Barthelmé, Trukenbrod, Engbert, and Wichmann (2013) introduced spatial point processes as a theoretical concept to gaze patterns and demonstrated how this helps to turn qualitative into quantitative questions. Here, we present a method from spatial statistics, i.e., the *pair correlation function* (PCF), to estimate spatial correlations between fixation locations during a trial in the presence of spatial inhomogeneity. Before applying the PCF to eye movement data during the first and second inspection of an image, we briefly describe the theoretical details of the PCF. We demonstrate (i) that the PCF provides rigorous statistical evidence for aggregation of fixation locations in single trials, (ii) that the PCF is differentially affected by a memory manipulation (first vs. second inspection

of an image), and (iii) that these differences can be explained by modulations of the attentional span within our SceneWalk model (Engbert et al., 2015).

Pair Correlation Function

We refer to Diggle (2013) for an introduction to the statistical analysis of point patterns and to Law et al. (2009) for a detailed description of the PCF and the successful application to plant ecology.

Computing the Pair Correlation Function

The density estimation of a point pattern, i.e., the probability of observing a point at a given location, is a first-order statistic for a spatial point process, which, therefore, plays the role of the mean value in classical statistics. In the upcoming sections we denote this first-order statistic as the intensity $\lambda(x)$. In the case of eye movements this represents the local average spatial density of fixations at a location x. Point patterns that are generated by a homogeneous point process are uniformly distributed and the underlying intensity $\lambda(x) = \lambda$ is constant for all x. For inhomogeneous point processes, where the 2D density of fixation locations is non-uniformly distributed, the intensity $\hat{\lambda}(x)$ is estimated for each location x separately, i.e.,

$$\hat{\lambda}(x) = \lim_{|dx|\to 0} \left\{ \frac{E[N(dx)]}{|dx|} \right\}. \tag{1}$$

Here, the density is given by the expected number of fixations falling into a disc of infinitesimal size $|dx|$. Note, the symbol $\hat{}$ is used to denote estimators.

While first-order statistics are concerned with locations of single points (ignoring spatial correlations), second-order statistics describe the relation between points. A crucial second-order statistic for the computation of PCFs is the pair density function $\rho(r)$. The pair density function represents the distribution of distances r between all pairs of points. Mathematically the pair density function $\hat{\rho}(r)$ is estimated by

$$\hat{\rho}(r) = \sum_{x_1, x_2 \in W}^{\neq} \frac{k(\|x_1 - x_2\| - r)}{2\pi r A_{\|x_1 - x_2\|}} \tag{2}$$

where k represents an Epanechnikov kernel, $\|x_1 - x_2\|$ denotes the displacement of two points, and $A_{\|x_1-x_2\|}$ is an edge-correction factor to counter the loss of pairs of points near the boundary of the inspection window especially for greater displacements $\|x_1 - x_2\|$.

Since the pair density function depends on the number of points, the PCF is computed as a normalized version of the pair density. The PCF is given by the intensity-weighted pair density function. In the case of a homogeneous PCF the pair density function is weighted by a constant at all distances, i.e.,

$$\hat{g}(r) = \frac{1}{\hat{\lambda}^2} \hat{\rho}(r). \tag{3}$$

However, fixation locations are not distributed homogeneously and show aggregation due to bottom-up, top-down, and systematic oculomotor factors. Fortunately, the PCF can be

computed for inhomogeneous processes by weighting the pair density function with the intensities $\hat{\lambda}(x_i)$ estimated for an inhomogeneous point process at each fixation location, i.e.,

$$\hat{g}^*(r) = \sum_{x_1,x_2 \in W}^{\neq} \frac{1}{\hat{\lambda}(x_1)\hat{\lambda}(x_2)} \hat{\rho}(r) \tag{4}$$

The resulting PCFs will be non-negative, $g(r) \geq 0$, at all distances r. Values of the PCF close to one, $g(r) \approx 1$, indicate that pairs of points at distance r are independent. Points at distance r occur solely due to the underlying intensity $\hat{\lambda}(x)$. For larger values, i.e., $g(r) > 1$, point patterns are more abundant at distance r than expected by the intensity $\hat{\lambda}(x)$. Thus, pairs of points at distance r interact and observing a point increases the probability of observing a point at distance r. Conversely, smaller values, $g(r) < 1$, reveal that points are less abundant than the spatial average at distance r. Observing a point reduces the likelihood of observing a second point at distance r.

Figure 1 illustrates the PCFs on the basis of three point patterns. In all examples we computed the PCF assuming a homogeneous point process with constant intensity $\lambda(x) = \lambda$ (cf. Eq. 3) since deviations from uniformity are easier to visualize. The same interpretation, however, can be applied to inhomogeneous PCFs. The first example shows a regular point pattern (left column). Visual inspection of the points indicate a grid-like arrangement. The distance between neighboring points is relatively constant. The resulting PCF (bottom row) summarizes this behavior. At short distances, $r < 4$, the PCF reveals a strong inhibitory of effect, $\hat{g}(r) \approx 0$. The existence of a point impedes the occurrence of other points within this radius. At medium distances, $4 < r < 6$, the PCF reveals aggregation of points, $g(r) > 1$. Observing a point boosts the occurrence of points at this distance. Hence, the grid-like appearance. At larger distances, $r > 6$, the PCF lends support to the hypothesis of independence of points, since $g(r) \approx 1$. We observe no long-range interaction of pairs of points and the distribution of distances can be explained by the assumed density distribution, $\lambda(x)$.

The second example (Fig. 1, central panels) shows a random point pattern. Points are distributed uniformly. The resulting PCF reveals the independence of points at all distances, $\hat{g}(r) \approx 1$. Note, the aggregation at short distances r is an artifact generated by the estimation process. Finally, the third example illustrates an aggregated point process (right panels). The PCF at short distances, $r < 2$, reveals aggregation, $\hat{g}(r) > 1$, while the PCF at longer distances reveals independence, $\hat{g}(r) \approx 1$. Thus, observing a point increases the likelihood of observing other points in close proximity. The occurrence of distant points can be explained by the uniform distribution.

Finally, deviations from randomness, i.e., $g(r) \neq 1$, can be summed up and serves as a useful summary statistic of the overall behavior:

$$\chi = \int_0^\infty (g(r) - 1)^2 dr. \tag{5}$$

In practical applications, the deviation from randomness χ is computed over a finite interval, e.g., $\int_a^b .dr$ with $a < b$.

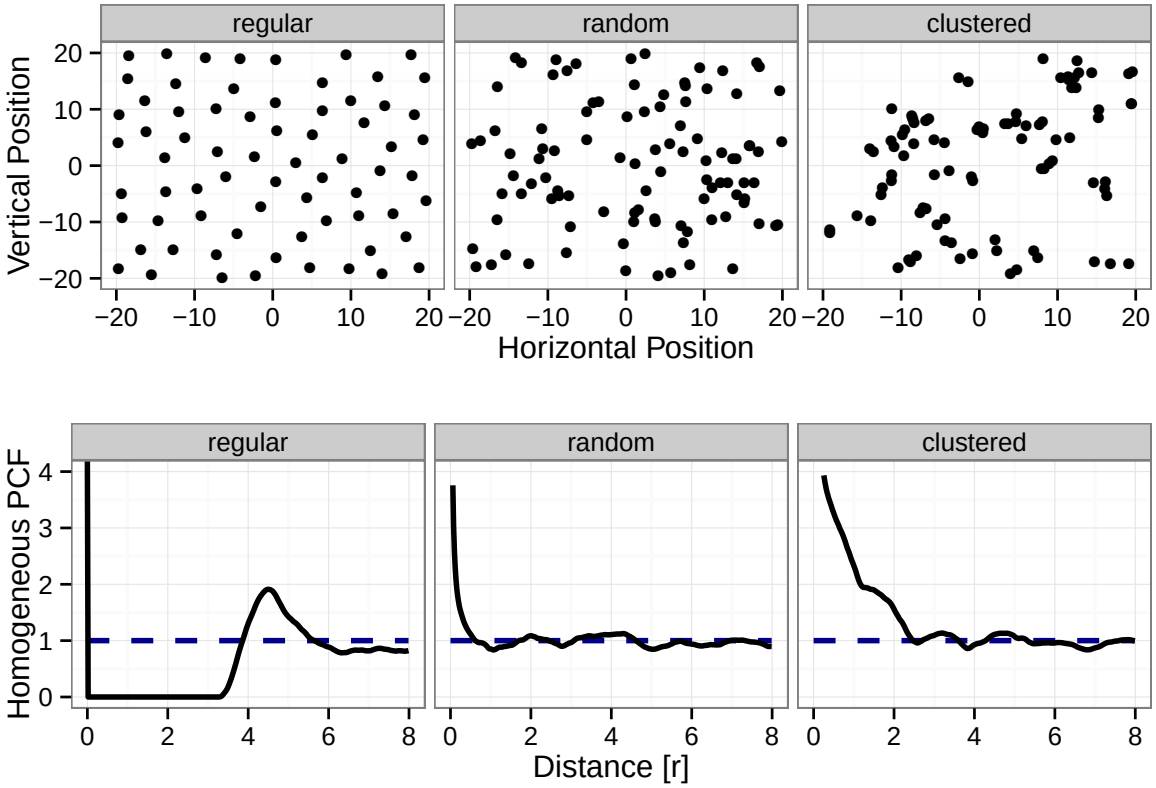

Figure 1. Examples of regular, random, and aggregated (clustered) point patterns (upper panels) and corresponding pair correlation functions (lower panels).

Application of the PCF to fixation locations

In this section we demonstrate how to compute the *pair correlation function* (PCFs) for eye movement data. The PCF disentangles effects due to dynamics inherent in a scanpath of a single observer from the overall inhomogeneity observed across observers. All analyses and graphs reported have been implemented in *R* using the *spatstat* (Baddeley & Turner, 2005; Baddeley, Rubak, & Turner, 2015) and *ggplot2* packages (Wickham, 2009). Computation of the PCF for fixation locations are done in three steps.

1. Simulate inhomogeneous and homogeneous control processes. We simulate two control point processes to evaluate our PCF computation. Figure 2 (left panel) shows fixations on an image from participants viewing the same scene for 10 seconds (see Methods for details). As expected fixation locations are not uniformly distributed and indicate inhomogeneity towards image boundaries. The intensity $\hat{\lambda}_s(x)$ of all fixation locations is depicted by gray shading where darker areas represent higher intensities. The smoothing bandwith for the intensity estimation was chosen as the average according to Scott's rule for bandwidth selection (R-function:

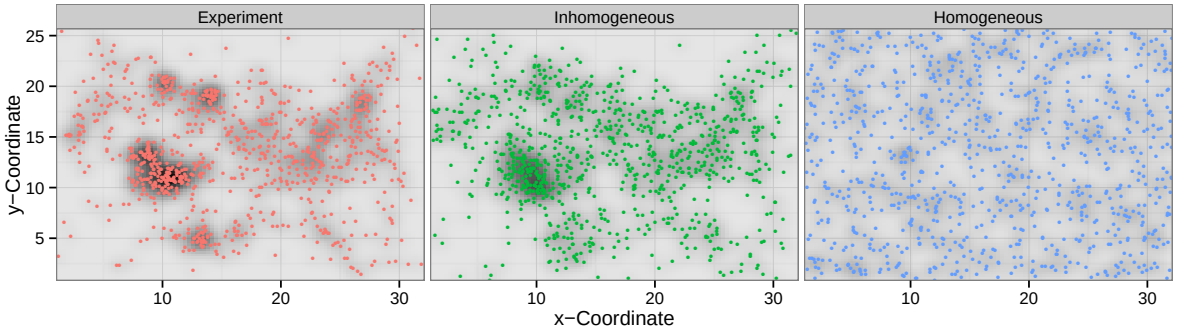

Figure 2. Distribution of fixation locations. Dots represent fixation locations, the estimated intensities of each point pattern is illustrated by gray shading. Experimental fixation locations (left panel), locations generated by a inhomogeneous point process (central panel), and a homogeneous point process (right panel).

`bw.scott`) from the *spatstat* package (Baddeley & Turner, 2005). We estimated an optimal bandwidth for each image. The estimated intensity $\hat{\lambda}_s(x)$ is used to simulate an inhomogeneous control point process. The inhomogeneous point process (central panel) samples points proportionally to the intensity $\hat{\lambda}_s(x)$. Hence, the resemblance of the experimental and simulated distributions. The homogeneous point process (right panel) assumes a uniform distribution of fixation locations across the entire image area, $\hat{\lambda}_s(x) = \lambda$. For every empirical scanpath we simulated one scanpath of equal length (same number of fixations) for the inhomogeneous point process and for the homogeneous point process obtained from Monte-Carlo simulations.

Examples of the empirical and simulated scanpaths are visualized in Figure 3. Each row shows matching scanpaths of the empirical, inhomogeneous and homogeneous point process. The estimated overall intensity of each point process on an image is displayed by gray shading. Fixations are likely to be located in areas of high average intensity $\hat{\lambda}(x)$. However, each sequence consists of a unique set of points where some scanpaths explore otherwise ignored locations or "miss" locations of high intensity (Fig. 3). Overall, scanpaths of the inhomogeneous and homogeneous point processes reveal less systematic exploration behavior than the empirical data. Hence, saccade amplitudes increase considerably.

2. Choose optimal bandwidth for intensity estimation of PCF. Next we need to choose an optimal bandwidth for estimation of the intensity $\hat{\lambda}(x)$ used to calculate the PCF $\hat{g}^*(r)$ (see Eq. 4). Since fixation locations in scanpaths of both control point processes are sampled independent from the preceding fixation history, average PCFs of both point processes are expected to reveal no spatial correlations, i.e. we expext $g(r) \approx 1$ at all distances r. We computed the deviation from randomness (Eq. 5) for PCFs computed with different bandwidths. We varied bandwidths from 0° and 10° in steps of 0.1° and computed the deviation from randomness for each scanpath. The average deviation at each bandwidth is plotted in Figure 4. Lines represent individual images. For all images, the deviation increases for small bandwidths and large bandwidths with an optimal bandwidth between 1.5° and 5°.

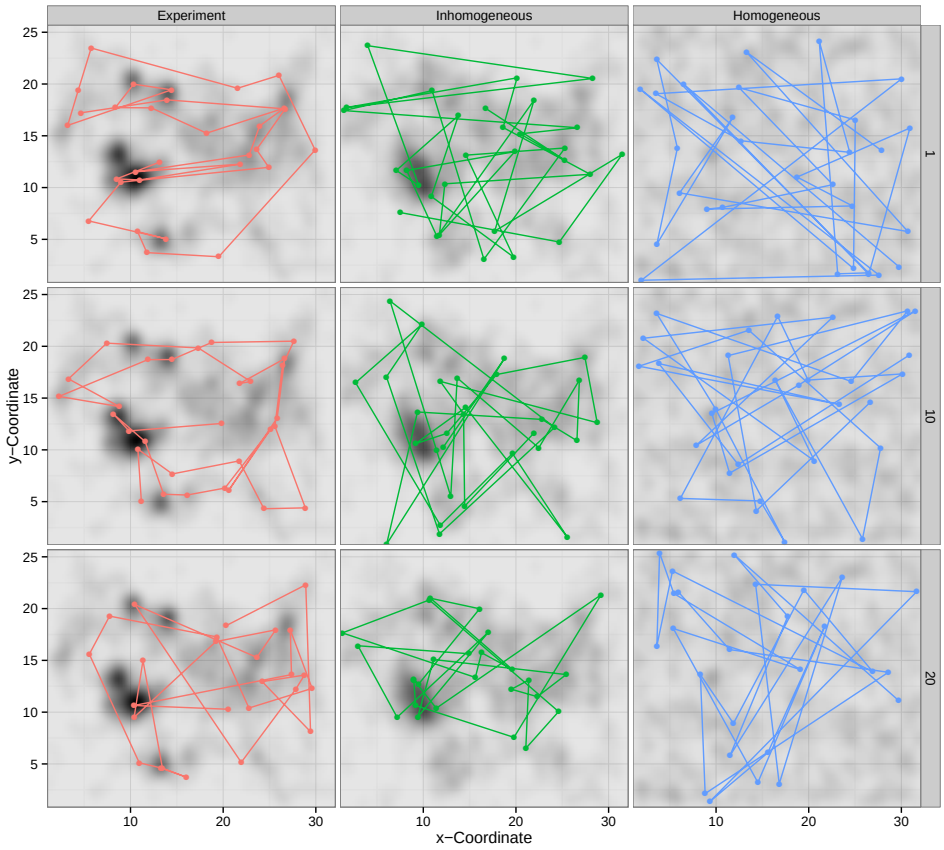

Figure 3. Three representative scanpaths during viewing of an image. Each row represents the scanpath during a single trials of the empirical data (red, left panel), the simulated inhomogeneous point process (green, central panel) and the simulated homogeneous point process (blue, right panel).

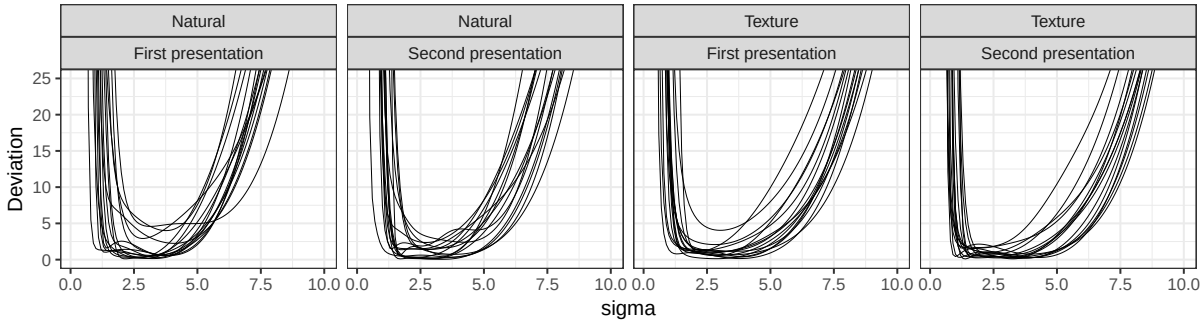

Figure 4. Optimal bandwidth for intensity estimation of PCF. The deviation from randomness (cf., Eq. 5) is evaluated for bandwidths between 0° and 10° for each image.

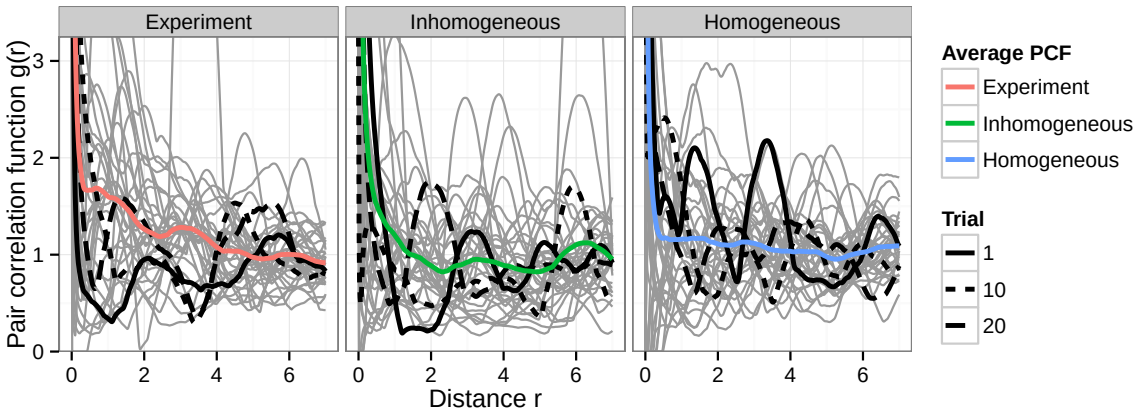

Figure 5. Pair correlation functions of individual scanpaths (gray lines) and the average PCF on an image (red line). Selected trials (Fig. 3) are displayed in black.

3. Compute PCF for each trial. In the last step we compute the PCF of our empirical data. For estimation, we use the intensity $\hat{\lambda}(x)$ that resulted in the smallest deviation from randomness of the PCF $\hat{g}^*(r)$ for the inhomogeneous point process (see previous step). PCFs of individual scanpaths on an image are displayed in Figure 5 (gray lines). The three example scanpaths from Figure 3 are plotted in black. PCFs vary strongly between individual trials for all point processes. The average empirical PCF across all scanpaths on an image (red line) deviates from randomness $\hat{g}^*(r) \neq 1$ for distances smaller than 4°. At distances beyond 4° the average PCF suggests independence of points, i.e., $\hat{g}(r) \approx 1$. Thus, fixations led to more fixations in close proximity during individual trials. Conversely, areas further away are fixated as predicted by chance, i.e., the overall inhomogeneity $\hat{\lambda}(r)$ observed across all participants. Inspection of the control point processes demonstrates the absence of spatial correlations for the control point processes. The average PCF of the inhomogeneous and homogeneous point process are constant with $\hat{g}^*(r) \approx 1$. The artifact of the estimation procedure at short distances is present in all estimates.

The same procedure can be repeated for each image. Figure 6 shows PCFs of each image (gray lines) as well as the average across all images (colored lines). While inhomogeneous and homogeneous point processes reveal no spatial correlations, empirical PCFs show spatial aggregation at short distances, $r < 4°$ in all conditions. For a more detailed discussion see the Results section.

Methods

Participants

We recorded eye movements of 35 participants (15 male, 20 female) aged 17–36 years (mean: 24.0). Participants received study credits or 8€ for participation and were recruited at the University of Postdam and from a local school (32 students, 3 pupils). All participants had

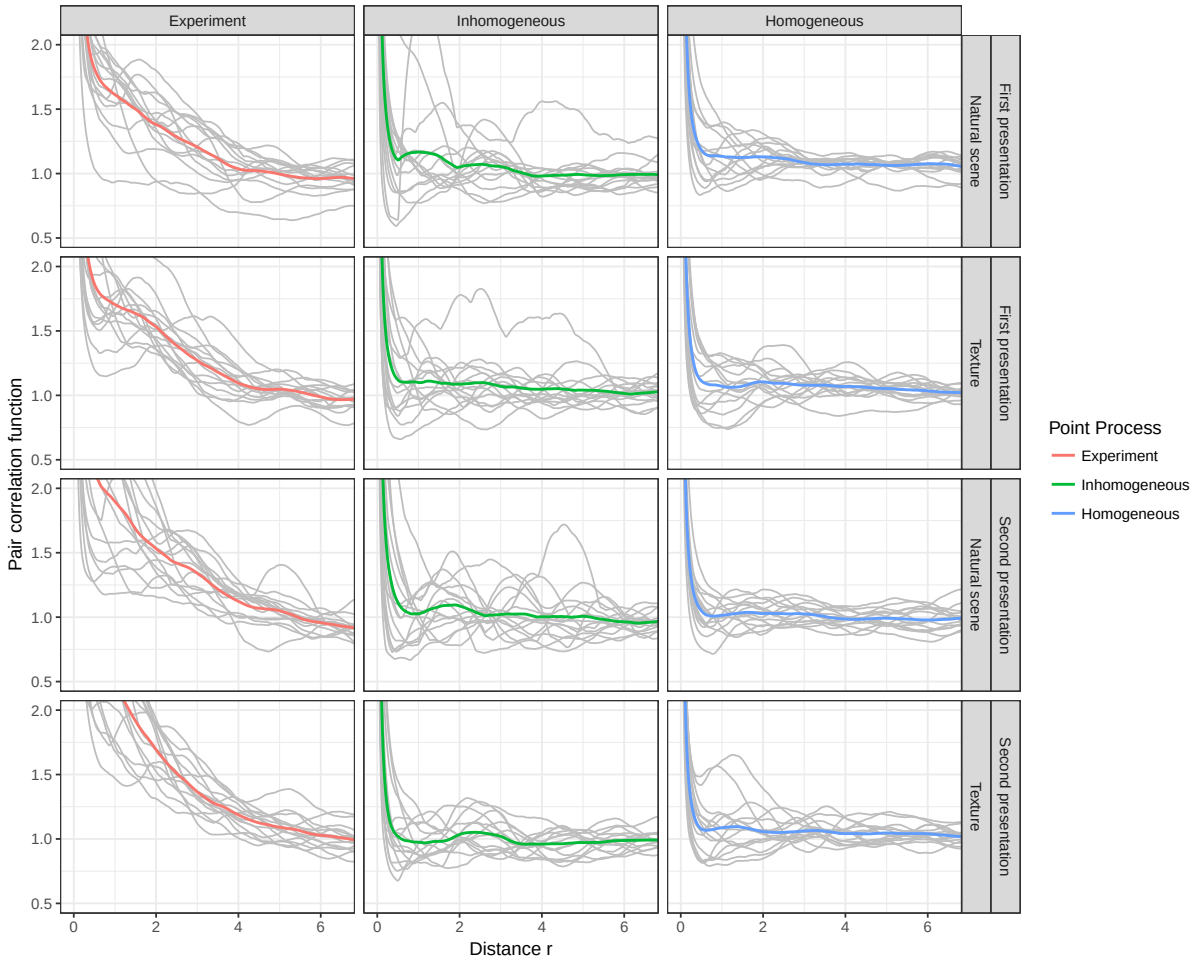

Figure 6. Pair correlation functions of individual images. PCFs were estimated for each condition separately (natural vs. texture images; first vs. second inspection). Estimated PCFs of the empirical fixation locations (red lines), and simulated locations generated by a inhomogeneous point process (green lines), and an homogeneous point process (blue lines).

normal or corrected-to-normal vision as assessed by the Freiburg Vision Test (FrACT; Bach, 1996).[1] The study conformed to the Declaration of Helsinki as well as national ethics guidelines. We obtained written informed consent from all participants.

Apparatus

Stimuli were presented on a 20" CRT monitor (Mitsubishi Diamond Pro 2070; refresh rate 120 Hz; resolution: 1280×1024 pixels). Eye movements were recorded binocularly using the video-based Eyelink 1000 system (SR Research, Osgoode, ON, Canada) with a sampling rate of 1000 Hz. In order to reduce head movements we asked participants to position their head on a chin-rest in front of the computer screen (viewing distance: 70 cm). Stimulus presentation and response collection were implemented in MATLAB (The MathWorks, Natick, MA, USA) using the Psychophysics Toolbox (PTB–3; Brainard, 1997; Kleiner et al., 2007; Pelli, 1997) and Eyelink Toolbox (Cornelissen, Peters, & Palmer, 2002).

Stimulus material

We used two sets of colored photographs in our experiment. In the first part of the experiment each set consisted of 15 images (Fig. 7). Image Set 1 contained photographs of natural landscapes and rural scenes. Image Set 2 contained photographs of textures. During the memory test in the second part of the experiment we added 15 images to each image set.

Task and procedure

Each trial began with the presentation of a black fixation cross in front of a uniform gray background. The fixation cross was placed at a random location within the image boundaries. After successful fixation, the fixation cross was replaced by the image for 10 s. Participants were instructed to explore each image for a subsequent memory test. The first block of the experiment consisted of 60 trials where each image was presented twice. Results from the first inspection of images have been described previously (Engbert et al., 2015). The second inspection has not been published earlier. In a second block participants completed a memory test with 60 trials. The memory test contained all presented images and thirty new images with natural scenes and textures. Participants had to judge whether the image had been presented during Block 1.

To minimize the potential influence of the monitor frame and since accuracy of eye trackers falls off towards the edges of a monitor, images were presented centrally with gray borders extending 32 pixels to the top/bottom and 40 pixels to the left/right of the image. The resulting size of the image was 1200×960 pixels (31.1°×24.9°).

Data preprocessing

We detected saccades by using a velocity-based algorithm (Engbert & Kliegl, 2003; Engbert & Mergenthaler, 2006). Saccades were defined as fast movements of both eyes that exceeded the average velocity during a trial by 6 standard deviations for at least 6 ms with a minimum amplitude of 0.5°. Eye traces between successive saccades were tagged as fixations. Fixation positions were computed by averaging the mean eye position of both eyes. Since trials started with a fixation check, first fixations on images were removed from the data set ($N = 2100$). In

[1] `http://michaelbach.de/fract/`

Figure 7. Images used in experiment. Left: natural scenes; right: texture images.

addition, fixations containing a blink or with a blink during an adjacent saccade were excluded from subsequent analyses ($N = 2214$). Overall, 55.526 fixations remained for further analyses.

SceneWalk model

For the interpretation of our results, we simulated fixation sequences with the SceneWalk model (Engbert et al., 2015; cf., Schütt et al., 2017). Fixation sequences are generated in the computational model by two competing activation maps: (i) an excitatory attention map that provides potential saccade targets and (ii) an inhibitory fixation map that tags previously fixated locations. Activations in the attention map a_{ij} at coordinates (i, j) evolve over time. Empirical saliency, i.e. the observed distribution of fixation locations, feeds into the attention map in our simulations. Thus, the empirical saliency is not restricted to purely bottom-up or top-down processing but contains all factors that contribute to the inhomogeneous distribution of fixation locations. Extraction from the empirical saliency is highest at fixation and decreases with increasing eccentricity. This corresponds to the attentional window of our model. Mathematically, the empirical saliency is weighted by a Gaussian envelope of size σ_1. Position of the attentional window a_{ij} changes after each saccade and remains constant otherwise. In addition leakage leads to a temporal decay of activations. The updating rule of the attention map a_{ij} is given by

$$a_{ij}(t+1) = \frac{\phi_{ij} A_{ij}(t)}{\sum_{kl} \phi_{kl} A_{kl}(t)} + (1-\rho) a_{ij}(t) \tag{6}$$

with the 2D-Gaussian $A_{ij}(t)$ centered upon fixation at time t, the empirical saliency ϕ_{ij}, and the rate of decay ρ. Dimension of maps in the model equals 128×128 ($k \times l$).

Temporal evolution of activations in the inhibitory map f_{ij} is very similar to the dynamics in the attention map a_{ij}. Temporal evolution consists of activation accumulation centered at fixation and a proportional temporal decay across the map. The updating rule of the fixation map f_{ij} is given by

$$f_{ij}(t+1) = F_{ij}(t) + (1-\omega) f_{ij}(t) \tag{7}$$

with a 2D-Gaussian $F_{ij}(t)$ with standard deviation σ_0 centered at fixation at time t and a decay rate of the fixation map ω. The fixation map tracks fixated areas and is motivated by inhibition of return (Klein & MacInnes, 1999) which has been suggested as a mechanism to drive exploration in scenes (Itti & Koch, 2001). Although the role of inhibition of return has been questioned (Smith & Henderson, 2009), model simulations support inhibitory tagging as an important mechansim during scene perception (Rothkegel et al., 2016; cf. Bays & Husain, 2012).

While attention and fixation map evolve independently over time, both maps are subsequently normalized and combined into a single map for target selection. The potential u_{ij} is given by

$$u_{ij}(t) = -\frac{[a_{ij}(t)]^{\lambda}}{\sum_{kl}[a_{kl}(t)]^{\lambda}} + \frac{[f_{ij}(t)]^{\gamma}}{\sum_{kl}[f_{kl}(t)]^{\gamma}} \tag{8}$$

where the exponents λ and γ are free parameters. Engbert et al. (2015) fixed these parameters to $\lambda = 1$ to reproduce the densities of gaze positions and $\gamma = 0.3$ to reproduce spatial correlations between fixation locations. We kept these values in our simulations. The probability of a location (i, j) to be chosen as the next saccade target can be extracted from the potential, i.e.

$$\pi_{ij}(t) = \max\left(\frac{u_{ij}(t)}{\sum_{(k,l)\in S} u_{kl}(t)}, \eta \right) \tag{9}$$

where S contains all positions on the grid with $u_{ij}(t) \leq 0$ and a free parameter η that adds noise to the selection process so that every position has at least a minimal probability to be chosen as the next saccade target. Target selection in the SceneWalk model occurs at the end of fixation where the eyes move instantaneously. The intervals between successive saccades were drawn from a gamma distribution of eighth order and a mean value of 275 ms.

Parameter estimation

Simulations were based on different parameters for each of the four experimental conditions (presentation × image type). As a starting point we used the parameters reported in Engbert et al. (2015). These parameters were estimated for fixations during the first presentation of natural

Table 1: Model parameters. Standard errors were calculated from five parameter estimations of the experimental data recorded during the first presentation of natural images.

		Natural Images		Texture Images		
	Parameter	First	Second	First	Second	Error
Attention span	σ_1	4.88	4.20	4.72	4.20	$\pm$0.11
Attention decay	$\log_{10}\rho$	-1.18	-1.18	-1.36	-1.36	$\pm$0.28
Inhibition span	σ_0	2.16	2.18	1.79	1.76	$\pm$0.25
Inhibition decay	$\log_{10}\omega$	-4.03	-4.03	-3.80	-3.80	$\pm$0.08
Noise	$\log_{10}\eta$	-4.04	-4.04	-4.51	-4.51	$\pm$0.07

images. We hypothesized that image type (natural scenes vs. textures) might affect target selection and decided to estimate all parameters for the first presentation of texture images anew. Previous work suggested that reinspection of images leads to a decreased attentional span (Kaspar & König, 2011a, 2011b). Hence, we decided to fix all parameters except for the sizes of the attention span σ_1 and inhibition span σ_0 for simulation of the second inspection of images. Parameter estimation was based on five images. Evaluation of parameters was based on all images (15 per image type). Limiting the analysis to the predicted images does not alter effects. A list of estimated parameter values can be found in Table 1.

Results

With our first analysis we expected to replicate the results of Kaspar and König (2011a, 2011b), i.e., second inspection of the same image leads to decreased saccade amplitudes. In addition, we investigated whether the two image types (natural scenes vs. textures) differentially affected saccade amplitudes. In a second analysis, we tested the sensitivity of the *pair correlation function* (PCF) to our experimental manipulations. All experimental results were compared to model simulations of the SceneWalk model (Engbert et al., 2015), the inhomogeneous and tghe homogeneous point processes discussed above.

Saccade amplitudes

Figure 8 shows average saccade amplitude on natural scenes (top) and texture images (bottom) during the first and second presentation. All simulated saccade amplitudes differed from the experimentally observed saccade amplitudes (all ts > 3; see appendix for details). However, saccades generated by the SceneWalk model were only slightly shorter than the experimentally observed saccades while saccade amplitudes from the inhomogeneous and homogeneous point processes were much larger. A linear mixed effects model (LME; Bates, Mächler, Bolker, & Walker, 2015) with random intercepts for subject and image revealed a significant fixed effect of Presentation but no effect of Image Type and no interaction in our experimental data (Tab. 2, left columns). Saccades were larger during the first inspection than during the second inspection. An LME model of the saccade amplitudes generated by the SceneWalk model replicated this effect qualitatively. However, the interaction of Presentation and Image Type also reached

significance. Saccade amplitudes were shorter on natural scenes than texture images during the second inspection. Both inhomogeneous and homogeneous point processes failed to generate any effects due to our experimental manipulations (all ts < 1.0).

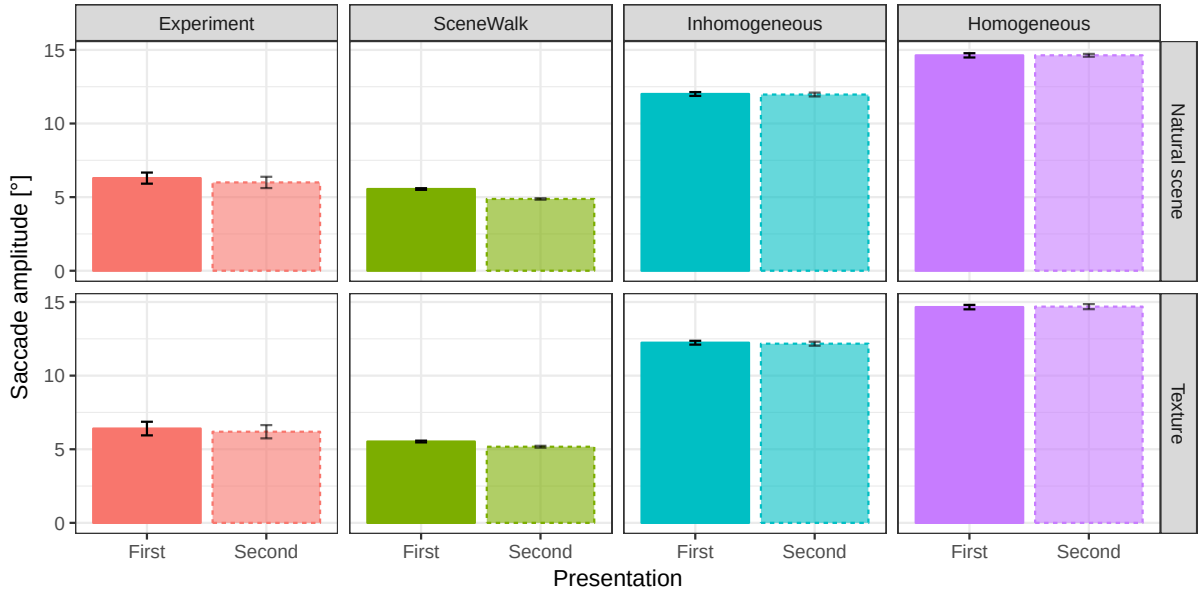

Figure 8. Saccade amplitudes. Experiment (red), and results of model simulations by the SceneWalk model (green), an inhomogeneous point process (blue), and an homogeneous point process (purple). Error bars represent 95% confidence intervals of participant variability.

Second order statistics: Pair correlation function

PCFs for each condition of the four point processes are plotted in Figure 9. We observed spatial correlations of fixation locations during individual trials in all conditions of our experimental data (red lines). Fixations locations were more abundant than expected by the overall inhomogeneity of fixation locations at short distances r. The PCF deviated from randomness, i.e., $\hat{g}^*(r) > 1$, at distances $r < 4°$. More importantly, the second presentation of an image (dashed lines) led to increased PCFs for both natural scenes (top row) and texture images (bottom row). Statistically, we evaluated spatial correlations by computing the deviation from randomness of each PCF, i.e., the summed deviation of the PCF from one for distances $0.5 \leq r \leq 6.5$ (Fig. 10; cf. Eq. 5). A linear mixed effect model (LME) with a random intercept for each image revealed a significant deviation from randomness (intercept), an effect of Presentation and of Image Type but no interaction. Thus, deviations were present in all conditions of our experimental data with larger deviations during the second inspection of an image and on texture images.

The SceneWalk model replicated this pattern of results qualitatively (Fig. 9, green lines). All conditions showed strong spatial correlations. PCFs deviated from randomness for distances $r < 6°$. The effect extended to larger distances in our model simulations. We analyzed deviations from randomness with another LME for the SceneWalk model (Tab. 2; cf. Fig. 10). PCFs

Table 2: Table of fixed effects of liner mixed effect models. We estimated separate models for saccade amplitudes and the summed deviation from randomness of the PCF for each point process. The table reports estimates of fixed effects (β) with standard errors (SE) and t values. ts>2 are interpreted as significant effects.

	Saccade amplitudes			PCF deviation		
	β	SE	t	β	SE	t
Experiment						
(Intercept)	6.225	0.205	30.31	130.76	8.721	14.99
Presentation	-0.128	0.018	-7.15	28.231	6.175	4.57
Image Type	0.091	0.056	1.63	19.555	8.721	2.24
Presentation × Image Type	0.018	0.018	1.02	4.230	6.175	0.69
SceneWalk						
(Intercept)	5.282	0.036	146.85	188.495	8.916	21.14
Presentation	-0.256	0.015	-16.72	59.708	8.916	6.70
Image Type	0.067	0.035	1.88	4.002	8.916	0.45
Presentation × Image Type	0.082	0.015	5.36	2.623	8.916	0.29
Inhomogeneous Point Process						
(Intercept)	12.090	0.114	106.21	12.002	6.765	1.77
Presentation	-0.024	0.027	-0.88	-10.138	5.687	-1.78
Image Type	0.109	0.113	0.96	-0.655	6.765	-0.10
Presentation × Image Type	-0.026	0.027	-0.96	-5.762	5.687	-1.01
Homogeneous Point Process						
(Intercept)	14.640	0.036	411.80	23.770	4.870	4.88
Presentation	0.001	0.031	<0.10	-10.799	2.992	-3.61
Image Type	0.029	0.032	0.90	2.642	4.870	0.54
Presentation × Image Type	0.021	0.031	0.70	8.076	2.992	2.70

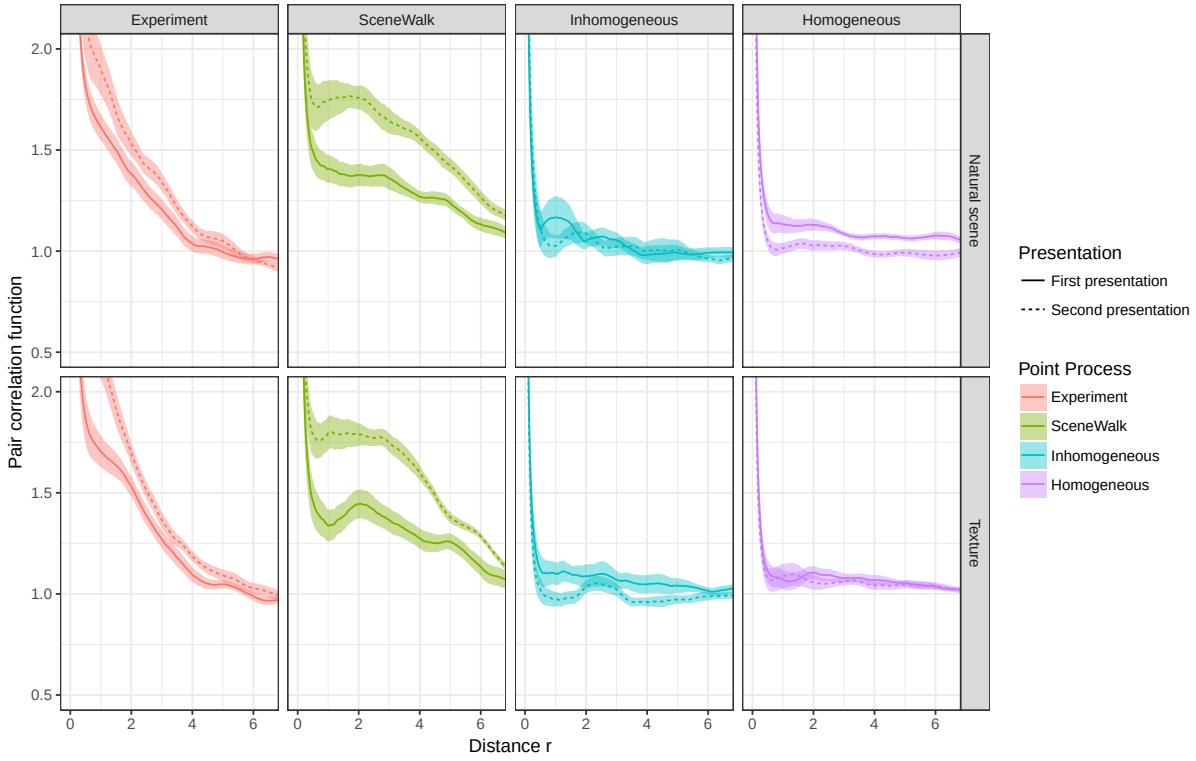

Figure 9. Average pair correlation functions (PCFs) for experimental and simulated point processes. PCFs were estimated for each condition separately (natural vs. abstract images; first vs. second inspection: solid vs. dashed lines). Estimated PCFs for the observed fixation locations (red lines), and simulated locations generated by the SceneWalk model (green lines), an inhomogeneous point process (blue lines), and an homogeneous point process (purple lines). 95% confidence intervals represent the variability across images.

deviated from randomness (intercept). The effect was larger for the second inspection. Texture images showed qualitatively larger deviations but this effect was not reliable. We observed no interaction of Presentation and Image Type in the deviation score of the SceneWalk model.

The PCFs of the inhomogeneous point process indicated no reliable spatial correlations, i.e., $\hat{g}^*(r) \approx 1$ at all distances (Fig. 9, blue lines). The absence of spatial correlations was expected, of course, since the optimal bandwidth λ for the estimation of the PCF was chosen to minimize the deviation from randomness of the inhomogeneous process (see Step 2 of the estimation process). This result was confirmed statistically by an LME on the deviation from randomness for the inhomogeneous point process (Tab. 2; cf. Fig. 10). There was no systematic deviation from randomness (intercept), as well as no effect due to Presentation and Image Type (all ts < 2).

PCFs of the homogeneous point process were similar to PCFs of the inhomogeneous point process, i.e., $\hat{g}^*(r) \approx 1$ at all distances (Fig. 9, purple lines). A LME on the deviation from randomness, however, revealed a small but reliable overall deviation from randomness (intercept), an effect of Presentation and a reliable interaction of Presentation and Image Type (Tab. 2;

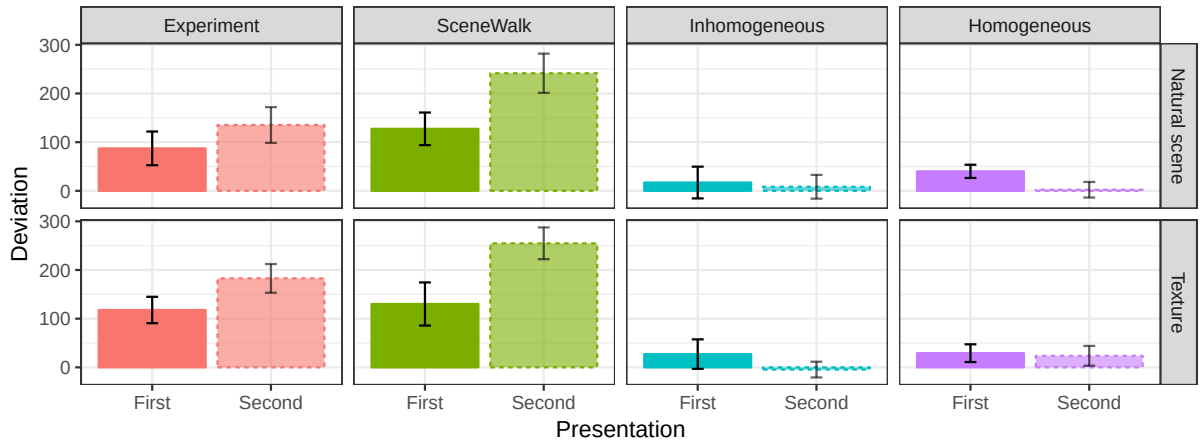

Figure 10. Summed deviation from randomness (Eq. 5) of empirical and simulated point processes for all conditions (natural vs. abstract images; first vs. second inspection). The deviation was computed for distances $0.5<r<6.5$. As expected, the deviation from randomness are smallest for the two control processes (homogeneous and inhomogeneous point process).

cf. Fig. 10). The effect of Presentation, however, was opposite to the effect observed in the experimental data and in the SceneWalk model with stronger deviations during the first presentation.

Discussion

During scene perception, fixations are not randomly distributed on an image. Instead fixations cluster in parts of an image due to bottom-up factors, top-down factors, and systematic tendencies of gaze control (Tatler & Vincent, 2008). We propose the *pair correlation function* (PCF) as a tool to investigate the relation of fixation positions within single trials and demonstrated that the PCF responds sensitively to a memory manipulation in our experiment. In addition, simulations of the SceneWalk model (Engbert et al., 2015) demonstrated that a reduced attentional span could explain the observed results on the PCF in a fully dynamical framework of scanpath generation.

Pair correlation function

Research on eye movements during scene perception has focused on the distribution of fixation locations across observers, as for example during the evaluation of saliency models (Bylinskii et al., 2015). However, this approach neglects dependencies between fixation locations during a trial (Engbert et al., 2015). The PCF is a method from spatial statistics to evaluate the relation of pairs of points (Diggle, 2013) and reveals whether points solely depend on the inhomogeneity of a point process or whether pairs of points affect each other mutually at a given distance r. The PCF can be applied to eye movement data (i.e., fixation locations) in three steps. In a first step, an inhomogeneous and homogeneous point processes needs to be simulated to evaluate the PCF estimation. Both point processes generate fixation locations that are independent at all

distances r. Hence, PCFs of both processes are expected to show no spatial correlations at any distance r. During a second step an optimal bandwidth needs to be chosen for the estimation of the PCF. As a criterion we suggest to use a bandwidth so that the PCF of the inhomogeneous point process has the least deviation from randomness, i.e. shows no spatial correlations. In a last step, the computed bandwidth can be used to compute PCFs for each individual trial.

In scene perception the PCF provides a measure whether fixation locations can be explained by the underlying distribution of all fixation locations (no spatial correlations between pairs of points) or whether fixation positions interact with each other at distance r. PCFs revealed spatial correlations of fixation locations in all conditions in our experimental data. Fixations were more abundant at distances $r < 4°$ than expected by the overall inhomogeneity of fixation locations. Beyond 4° fixation locations were independent of each other. Thus, observing a fixation increased the probability of observing more fixations than expected by the overall inhomogeneity within 4°. Beyond 4° fixations were as likely as predicted by the local intensity of fixation locations. As expected, neither the inhomogeneous nor the homogeneous point process revealed strong spatial correlations since fixation locations were independent of each other for these point processes. Therefore, aggregation observed in our PCFs was not the result of the estimated intensity λ of the 2D fixation density.

Repeated presentation of images

To test the sensitivity of the PCF, we recorded eye movements of participants while viewing an image twice. The repeated presentation was expected to result in shorter saccade amplitudes due to a reduced attentional window (Kaspar & König, 2011a, 2011b). We replicated shorter saccade amplitudes during the second inspection independent of image type. In addition, we observed stronger spatial correlations within 4° during the second inspection, in particular on texture images. Thus, the PCF seemed to be a bit more sensitive towards our experimental manipulation of Image Type. This further supported the usefulness of the PCF as a method to characterize eye movement behavior.

Reduced saccade amplitudes as well as increased aggregation might be generated by a reduced attentional span (Kaspar & König, 2011a, 2011b). We tested this hypothesis with simulations of the computational SceneWalk model (Engbert et al., 2015). Parameter estimation led to a reduced attentional span in the SceneWalk model during the second inspection of images which in turn led to shorter saccade amplitudes and stronger aggregation of fixation locations as quantified by the PCFs. Hence, our simulation results are in agreement with the interpretation of a reduced attentional span during repeated inspection of images.

In its current form the SceneWalk model overestimates aggregation in particular during the second inspection. However, our results are predictions and are not optimized to account for the experimentally observed PCFs. Beside the size of the aggregation, we observed a difference in the functional form of the PCF. PCFs of the SceneWalk model did not decrease as fast as expected by the experimental data. This might have been a result of the Gaussian form of our attentional window. A revision of the model using a modified attentional window might improve model fit in this respect (cf., Schütt et al., 2017).

Relation to fixation durations

Due to their partial independence (Findlay & Walker, 1999) fixation locations and fixation durations have successfully been studied in isolation. However, in tasks like scene perception interest is growing to understand the interaction of fixation locations and fixation durations. Interestingly, spatial statistics provides an extension of the PCF that includes covariates, so called *marks*. The *mark correlation function* (MCF) weights the PCF with its marks and reveals interactions between the PCF and its marks. In the case of eye movements, fixation durations can be used as marks. The combined analysis in form of the MCF might provide a useful tool for a better understanding of the interaction of fixation locations and fixation durations as well as for the evaluation of computational models that combine spatial control (e.g., Engbert et al., 2015) and temporal control (e.g., Laubrock, Cajar, & Engbert, 2013; Trukenbrod & Engbert, 2014).

Conclusions

The *pair correlation function* (PCF) is a powerful tool to analyze spatial correlations of fixation locations. During scene perception the PCF reveals aggregation of fixations during individual trials and reacts differentially to experimental manipulations. Simulations of a computational model demonstrate that a reduced attentional span leads to increased aggregation of fixation locations. Our work provides an example how spatial statistics and computational modeling can be combined to investigate general statistical properties of eye movement control.

Acknowledgments

This work was supported by Deutsche Forschungsgemeinschaft (grants EN 471/13–1 to R.E.) and by Bundesministerium für Bildung und Forschung (BMBF) via Bernstein Center for Computational Neuroscience Berlin (Project B3, Förderkennzeichen 01GQ1001F to R.E.).

References

Bach, M. (1996). The freiburg visual acuity test–automatic measurement of visual acuity. *Optometry & Vision Science*, *73*(1), 49–53.

Baddeley, A., Rubak, E., & Turner, R. (2015). *Spatial point patterns: Methodology and applications with r*. Boca Raton: CRC Press. doi: 10.18637/jss.v075.b02

Baddeley, A., & Turner, R. (2005). spatstat: An R Package for Analyzing Spatial Point Patterns. *Journal of Statistical Software*, *12*(i06), 1–42.

Ballard, D. H., Hayhoe, M. M., & Rao, R. P. N. (1997). Deictic codes for the embodiment of cognition. *Behavioral & Brain Sciences*, *20*(4), 723–767.

Barthelmé, S., Trukenbrod, H. A., Engbert, R., & Wichmann, F. A. (2013). Modeling fixation locations using spatial point processes. *Journal of Vision*, *13(12):1*, 1—-34.

Bates, D., Mächler, M., Bolker, B., & Walker, S. (2015). Fitting linear mixed-effects models using lme4. *Journal of Statistical Software*, *67*(1), 1–48. doi: 10.18637/jss.v067.i01

Bays, P. M., & Husain, M. (2012). Active inhibition and memory promote exploration and search of natural scenes. *Journal of Vision*, *12*(8), 1–8. doi: 10.1167/12.8.8

Borji, A., Sihite, D. N., & Itti, L. (2013). Objects do not predict fixations better than early saliency: A re-analysis of Einhäuser et al.'s data. *Journal of Vision*, *13(10):18*, 1–4.

Brady, T. F., Konkle, T., Alvarez, G. A., & Oliva, A. (2008). Visual long-term memory has a massive storage capacity for object details. *Proceedings of the National Academy of Sciences*, *105*(38), 14325–14329.

Brainard, D. H. (1997). The Psychophysics Toolbox. *Spatial Vision*, *10*, 443–446.

Bruce, N. D. B., & Tsotsos, J. K. (2009). Saliency, attention, and visual search: An information theoretic approach. *Journal of Vision*, *9(3):5*, 1–24.

Bylinskii, Z., Judd, T., Borji, A., Itti, L., Durand, F., Oliva, A., & Torralba, A. (2015). *MIT Saliency Benchmark.* http://saliency.mit.edu/.

Castelhano, M. S., Mack, M. L., & Henderson, J. M. (2009). Viewing task influences eye movement control during active scene perception. *Journal of Vision*, *9(3):6*, 1–15.

Cerf, M., Harel, J., Einhäuser, W., & Koch, C. (2007). Predicting human gaze using low-level saliency combined with face detection. *Advances in Neural Information Processing Systems*, *20*, 241–248.

Cornelissen, F. W., Peters, E., & Palmer, J. (2002). The Eyelink Toolbox: Eye tracking with MATLAB and the Psychophysics Toolbox. *Behavior Research Methods, Instruments & Computers*, *34*, 613–617.

Diggle, P. J. (2013). *Statistical analysis of spatial and spatio-temporal point patterns.* Boca Raton, FL: CRC Press.

Einhäuser, W., Spain, M., & Perona, P. (2008). Objects predict fixations better than early saliency. *Journal of Vision*, *8(14):18*, 1–26.

Engbert, R., & Kliegl, R. (2003). Microsaccades uncover the orientation of covert attention. *Vision Research*, *43*, 1035–1045.

Engbert, R., & Mergenthaler, K. (2006). Microsaccades are triggered by low level retinal image slip. *Proceedings of the National Academy of Sciences USA*, *103*, 7192–7197.

Engbert, R., Trukenbrod, H. A., Barthelmé, S., & Wichmann, F. A. (2015). Spatial statistics and attentional dynamics in scene viewing. *Journal of vision*, *15(1):14*, 1—-17.

Findlay, J. M., & Walker, R. (1999). A model of saccade generation based on parallel processing and competitive inhibition. *Behavioral & Brain Sciences*, *22*, 661–721.

Foulsham, T., & Kingstone, A. (2010). Asymmetries in the direction of saccades during perception of scenes and fractals: Effects of image type and image features. *Vision Research*, *50*(8), 779–795.

Foulsham, T., Kingstone, A., & Underwood, G. (2008). Turning the world around: Patterns in saccade direction vary with picture orientation. *Vision Research*, *48*(17), 1777–1790.

Hayhoe, M., & Ballard, D. (2005). Eye movements in natural behavior. *Trends in Cognitive Sciences*, *9*(4), 188–194.

Hollingworth, A., & Henderson, J. M. (2002). Accurate visual memory for previously attended objects in natural scenes. *Journal of Experimental Psychology: Human Perception & Performance*, *28*(1), 113–136.

Hollingworth, A., Williams, C. C., & Henderson, J. M. (2001). To see and remember: Visually specific information is retained in memory from previously attended objects in natural scenes. *Psychonomic Bulletin & Review*, *8*(4), 761–768.

Hooge, I. T. C., Over, E. A. B., van Wezel, R. J. A., & Frens, M. A. (2005). Inhibition of return is not a foraging facilitator in saccadic search and free viewing. *Vision Research*, *45*(14), 1901–1908.

Itti, L., & Koch, C. (2001). Computational modelling of visual attention. *Nature Reviews Neuroscience*, *2*(3), 194–203.

Judd, T., Ehinger, K., Durand, F., & Torralba, A. (2009). Learning to predict where humans look. In *Computer vision, 2009 ieee 12th international conference on* (pp. 2106–2113).

Kaspar, K., & König, P. (2011a). Overt attention and context factors: The impact of repeated presentations, image type, and individual motivation. *PLoS ONE*, *6*(7), e21719.

Kaspar, K., & König, P. (2011b). Viewing behavior and the impact of low-level image properties across repeated presentations of complex scenes. *Journal of Vision*, *11(13):26*, 1–29.

Kienzle, W., Franz, M. O., Schölkopf, B., & Wichmann, F. A. (2009). Center-surround patterns emerge as optimal. *Journal of Vision*, *9(5):7*, 1–15.

Klein, R. M., & MacInnes, W. J. (1999). Inhibition of return is a foraging facilitator in visual search. *Psychological Science*, *10*(4), 346–352.

Kleiner, M., Brainard, D., Pelli, D., Ingling, A., Murray, R., & Broussard, C. (2007). What's new in psychtoolbox–3. *Perception*, *36*(ECVP Abstract Supplement).

Koch, C., & Ullman, S. (1985). Shifts in visual attention: Towards the underlying circuitry. *Human Neurobiology*, *4*, 219–222.

Kümmerer, M., Wallis, T. S. A., & Bethge, M. (2016). Deepgaze II: reading fixations from deep features trained on object recognition. *CoRR*, *abs/1610.01563*. Retrieved from `http://arxiv.org/abs/1610.01563`

Land, M. F., & Hayhoe, M. (2001). In what ways do eye movements contribute to everyday activities? *Vision Research*, *41*(25-26), 3559–3565.

Laubrock, J., Cajar, A., & Engbert, R. (2013). Control of fixation duration during scene viewing by interaction of foveal and peripheral processing. *Journal of Vision*, *13*((12):11). doi: doi: 10.1167/13.12.11

Law, R., Illian, J., Burslem, D. F. R. P., Gratzer, G., Gunatilleke, C. V. S., & Gunatilleke, I. A. U. N. (2009). Ecological information from spatial patterns of plants: insights from point process theory. *Journal of Ecology*, *97*(4), 616–628.

Le Meur, L., & Liu, Z. (2015). Saccadic model of eye movements for free-viewing condition. *Vision Research*, *in press*.

Mannan, S. K., Ruddock, K. H., & Wooding, D. S. (1997). Fixation patterns made during brief examination of two-dimensional images. *Perception*, *26*(8), 1059–1072.

Melcher, D. (2001). Persistence of visual memory for scenes. *Nature*, *412*(6845), 401–401.

Melcher, D., & Kowler, E. (2001). Visual scene memory and the guidance of saccadic eye movements. *Vision Research*, *41*(25-26), 3597–3611.

Nuthmann, A., & Henderson, J. M. (2010). Object-based attentional selection in scene viewing. *Journal of Vision*, *10(8):20*, 1–19.

Parkhurst, D., Law, K., & Niebur, E. (2002). Modeling the role of salience in the allocation of overt visual attention. *Vision Research*, *42*(1), 107–123.

Pelli, D. G. (1997). The videotoolbox software for visual psychophysics: Transforming numbers into movies. *Spatial Vision*, *10*, 437–442.

Pelz, J. B., & Canosa, R. (2001). Oculomotor behavior and perceptual strategies in complex tasks. *Vision Research*, *41*(25-26), 3587–3596.

Reinagel, P., & Zador, A. M. (1999). Natural scene statistics at the centre of gaze. *Network: Computation in Neural Systems*, *10*, 341–350.

Rothkegel, L. O., Trukenbrod, H. A., Schütt, H. H., Wichmann, F. A., & Engbert, R. (2016). Influence of initial fixation position in scene viewing. *Vision Research*, *129*, 33–49. doi: http://dx.doi.org/10.1016/j.visres.2016.09.012

Schütt, H. H., Rothkegel, L., Trukenbrod, H. A., Reich, S., Wichmann, F. A., & Engbert, R. (2017). Likelihood-based parameter estimation and comparison of dynamical cognitive models. *arXiv*.

Smith, T. J., & Henderson, J. M. (2009). Facilitation of return during scene viewing. *Visual Cognition*, *17*(6-7), 1083–1108.

Standing, L. (1973). Learning 10000 pictures. *The Quarterly Journal of Experimental Psychology*, *25*(2), 207–222.

Standing, L., Conezio, J., & Haber, R. N. (1970). Perception and memory for pictures: Single-trial learning of 2500 visual stimuli. *Psychonomic Science*, *19*(2), 73–74.

Stoll, J., Thrun, M., Nuthmann, A., & Einhäuser, W. (2015). Overt attention in natural scenes: Objects dominate features. *Vision Research*, *107*, 36–48.

Tatler, B. W. (2007). The central fixation bias in scene viewing: Selecting an optimal viewing position independently of motor biases and image feature distributions. *Journal of Vision*, *7(14):4*, 1–17.

Tatler, B. W., Baddeley, R. J., & Gilchrist, I. D. (2005). Visual correlates of fixation selection: Effects of scale and time. *Vision Research*, *45*(5), 643–659.

Tatler, B. W., & Vincent, B. T. (2008). Systematic tendencies in scene viewing. *Journal of Eye Movement Research*, *2*(2), 1–18.

Torralba, A., Oliva, A., Castelhano, M. S., & Henderson, J. M. (2006). Contextual guidance of eye movements and attention in real-world scenes: The role of global features in object search. *Psychological Review*, *113*(4), 766–786.

Trukenbrod, H. A., & Engbert, R. (2014). ICAT: A computational model for the adaptive control of fixation durations. *Psychonomic Bulletin & Review*, *21*(4), 907–934.

Vig, E., Dorr, M., & Cox, D. (2014). Large-scale optimization of hierarchical features for saliency prediction in natural images. *Computer Vision and Pattern Recognition*, 2798–2805.

Wickham, H. (2009). *ggplot2: elegant graphics for data analysis*. Springer New York. Retrieved from `http://had.co.nz/ggplot2/book`

Wilming, N., Harst, S., Schmidt, N., & König, P. (2013). Saccadic momentum and facilitation of return saccades contribute to an optimal foraging strategy. *PLoS Computational Biology*, *9*(1), e1002871.

Yarbus, A. L. (1967). *Eye movements and vision*. Plenum Press.

Zhang, L., Tong, M. H., Marks, T. K., Shan, H., & Cottrell, G. W. (2008). SUN: A Bayesian framework for saliency using natural statistics. *Journal of Vision*, *8(7):32*, 1–20.